Modern Physics Letters B
Vol. 28, No. 26 (2014) 1450205 (10 pages)

DOI: 10.1142/S0217984914502054

Influence of the probe-sample interaction angle on image formation in apertureless scanning near field optical microscope

J. M. Merlo*, V. Coello†,¶, R. Cortés†, J. F. Aguilar‡ and A. Flores-Rosas§

*Department of Physics, Boston College,
140 Commonwealth Avenue, Chestnut Hill, Massachusetts 02467, USA
†Centro de Investigación Científica y de Educación Superior de Ensenada Unidad Monterrey,
Alianza Sur No. 105, Nueva Carretera Aeropuerto Km 9.5 Parque de Investigación e
Innovación Tecnológica (PIIT), Apodaca, C. P. 66629, N. L., México
‡Instituto Nacional de Astrofísica Óptica y Electrónica,
Luis Enrique Erro No. 1, Sta. Ma. Tonantzintla, Puebla, C. P. 72840, Pue, México
§División de Ingenierías, Campus Irapuato-Salamanca, Universidad de Guanajuato,
Carretera Salamanca-Valle de Santiago Km 3.5 and 1.8, Comunidad de Palo Blanco,
Apartado Postal 215-A, Salamanca, Gto., México
¶vcoello@cicese.mx

Received 25 April 2014
Revised 1 August 2014
Accepted 9 September 2014
Published 8 October 2014

Using the two-dimensional finite difference time domain method, we report on the image formation of an apertureless scanning near field optical microscope. It is found that the obtained images are influenced by the angle at which the probe interacts with a dielectric sample under total internal reflection illumination. The scanning probe is assumed to be a sharp silver tip with similar shape to those used in atomic force microscopy. We show that the near-field optical response produced by semi-circular and square imperfections are significantly affected with small (0°–10°) variations of the probe-sample interaction angle.

Keywords: Apertureless SNOM; near field artifacts; two-dimensional FDTD.

1. Introduction

Since the apertureless scanning near field optical microscope (a-SNOM) was first reported,[1,2] several works have been devoted to show its capabilities and applications.[3–8] The a-SNOM is a well-known technique that, by imaging in the optical near-field region, can extend the resolution of the optical microscope beyond the diffraction limit. The fundaments of the a-SNOM are found in the detection of evanescent waves[9] which contain information about the high spatial frequencies of

¶Corresponding author.

the surface profile. Here, the optical resolution is primarily determined by the size tip in the extreme end of a probe.[10] Then, in order to get high optical resolutions, it is necessary to have a very sharp tip.[10] An a-SNOM combined with a shear force microscope has proved to be a powerful tool to investigate, simultaneously, the topography and the optical response of a surface on a sub-wavelength scale.[11] However, the interpretation of such imaging system measurements can be rather complicated, even in a commercial unit, because of the influence of the probe on the field map.[12] The problem becomes critic when the tip is either acting as a perturbative probe[13] of the optical fields or influencing the contrast of the recorded image.[14] In this context, recently, we have reported on the angle dependence of the interaction distance in the shear-force technique.[15] We have found an exponential dependence of the interaction distance on the approaching angle. This exponential dependence may induce another kind of artifact. The angle dependence of the normal Casmir force between a corrugated plate and corrugated sphere has also been experimentally demonstrated.[16] Casimir and Van der Waal forces as well as capillary force from environment humidity are generally accepted as possible explanations for the origin of the shear forces. From the abovementioned, it is clear that careful and systematic studies conducted to strongly reduce the influence (on the near-field optical image) of the different kind of artifacts[12] are still needed. In order for a-SNOM to become a competitive technique, with respect to others scanning probe microscopy methods, several criteria for a-SNOM artifact-free imaging have been reported[17,18] including evanescent illumination using total internal reflection.[19] Furthermore, numerical simulations have also contributed to a certain understanding of the whole physical process involved in the probe-sample interaction of this kind of microscopy. The finite difference time domain (FDTD), proposed by Yee,[20] has demonstrated to be a very powerful tool for studying interactions at such small scales, even in three dimensions.[21] In fact, recent works, based in FDTD simulations, were oriented to the design of nanostructures with desired optical functionalities.[21–23] Here, using a two-dimensional FDTD method, we investigate the influence of the probe-sample interaction angle on the near-field optical response of nano-objects which are illuminated under total internal reflection. The scattered field, for an a-SNOM configuration, was simulated as a function of the interaction angle for, both, a semi-circular and a rectangular nano-object surface defect. The simulations exhibited features that suggest that the near-field intensity distributions depend on the interaction probe-sample angle. This artifact may compromise the interpretation of a-SNOM image as well as the estimation of its optical resolution.

2. Methodology

The spatial resolution is probably the single most important factor that determines the quality of an a-SNOM image. The measurement of the spatial resolution of the a-SNOM instrument has been typically estimated by using several standard calibration samples such as polystyrene latex spheres,[24] and square dielectric

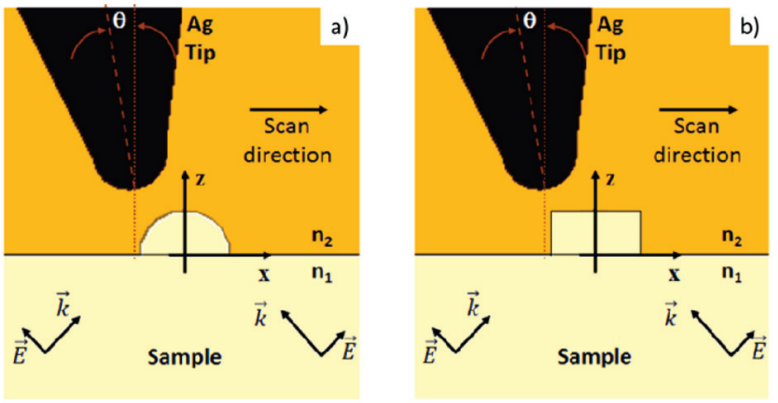

Fig. 1. (Color online) Scheme of the simulation areas. The incident field is produced by two counter propagating plane waves with wavelength of 650 nm in TM polarization. The circular imperfection is showed on (a) and the rectangular on (b).

gratings.[25] Bearing these geometries in mind, two set of calculations were considered: A semi-circular imperfection with various diameter sizes [Fig. 1(a)], and a rectangular imperfection with different areas [Fig. 1(b)]. In both cases, the imperfections are immerse in the glass medium and centered at the reference system. The probe-sample interaction angle, θ, is defined as the angle generated between the tip axis and the normal direction [Figs. 1(a) and 1(b)]. Ideally, in order to directly relate these results to experimental work using this type of probe-sample interactions, we would like to investigate a sample containing a large number of arbitrary-shaped defects. In general, this problem is very complicated, and even a fairly simple case of an irregular surface defect requires elaborated numerical simulations.[26]

Instead, as it was described before, we consider several series of related simple examples. While each of these cases consists of specific introduced defects, the number of calculated angles is large enough to ensure the reliability of obtained data. Furthermore, the ensemble of cases is chosen to illustrate important general trends that can be extrapolated to draw some qualitative conclusions about imperfections on a real sample surface. The dimension of the calculated area was 100×100 nm^2 with a mesh size of 0.5×0.5 nm^2 [Figs. 1(a) and 1(b)]. In a-SNOM, the evanescent signal is scattered, by a vibrating probe, toward a photodetector which averages the intensity of the optical field. Therefore, we calculated the averaged intensity field over the total area of the image. We begin with the calculation of the electromagnetic field distribution around the tip subject to standing evanescent wave illumination that was created in a glass/air interface by two counter-propagating totally internally reflected waves with equal amplitudes. The incident light is TM polarized with a free space wavelength, $\lambda = 650$ nm and having an incidence angle of 45°. The refractive index of the glass and air are assumed to be $n_1 = 1.52$ and $n_2 = 1$, respectively. The scan is toward the positive X-axis direction [Figs. 1(a)

and 1(b)], with a step size of 5 nm and a constant height, CH = 15 nm. For a-SNOM configuration, the probe must be placed very close to the sample, i.e. at a CH $\ll \lambda/2$. In our case, we use a CH $\approx \lambda/40$ which is small enough to ensure true near field optical contrast. The silver tip has a refractive index of $0.05222 + 4.4094i$ (Ref. 27) and a diameter (at its very end) of 20 nm. The shape and dimensions of the tip are similar to those used in atomic force microscopy (AFM).[28] The calculated semi-circular diameters were 10, 25, 50 and 100 nm, whereas the rectangular widths were 5, 12.5, 25 and 100 nm with heights of 10, 25, 50 and 100 nm, respectively. Note that the considered structures dimensions are in the range of 10–100 nm, which are typical sizes for nanometer-scale physical studies.

3. Results and Discussion

For the case of the semi-circular imperfections of Fig. 1(a), we calculated the intensity profiles along the X-axis as a function of θ [Figs. 2(a)–2(d)].

Thus, as the probe tip scans the surface, changes in the optical signal can be produced which are related with the optical properties of the sample volume just below the tip. The local optical response of the surface imperfection can be determined with a lateral resolution essentially given by the effective apex radius. In the case of the 10 nm diameter semi-circular imperfection, since the imperfection size

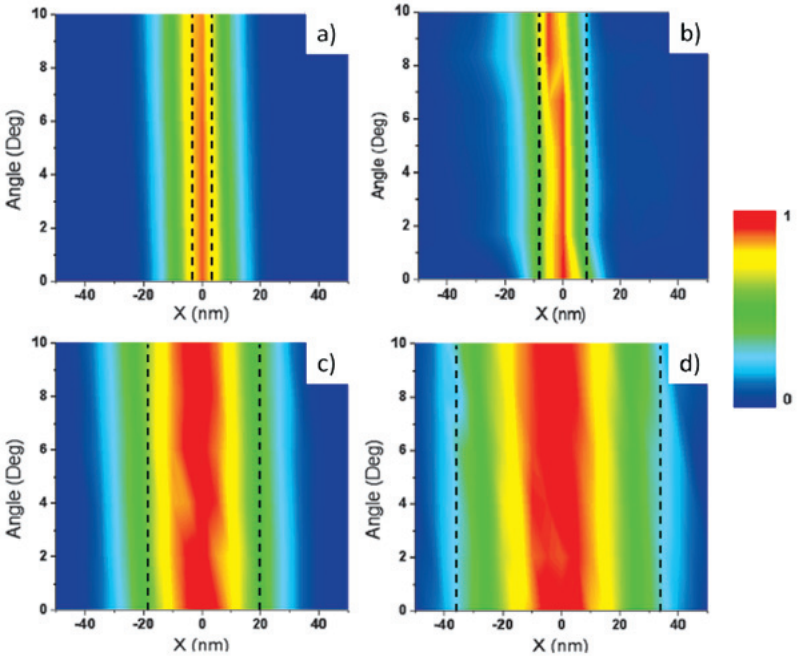

Fig. 2. (Color online) Average intensity obtained at different positions of the X-direction as a function of the interaction angle for a semi-circular imperfection of diameter. (a) 10 nm, (b) 25 nm, (c) 50 nm and (d) 100 nm. The dashed lines indicate the width in the absence of the tip.

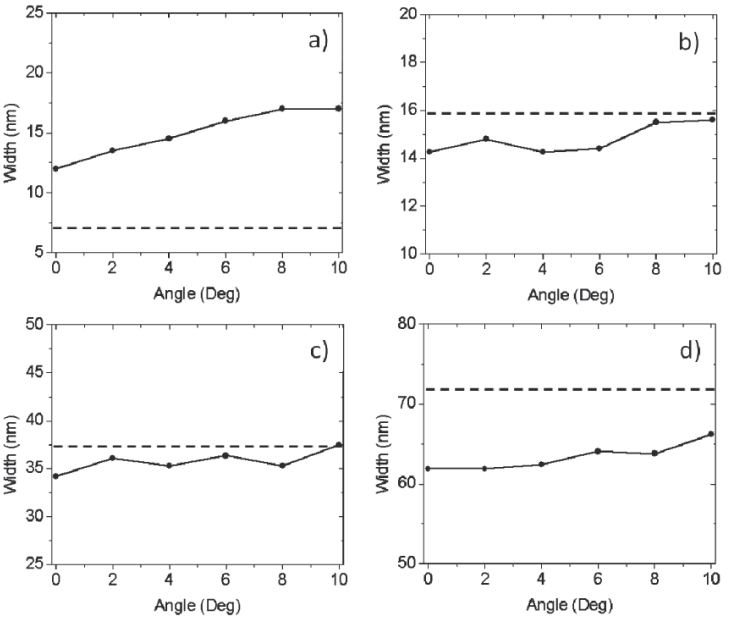

Fig. 3. Width measured at FWHM in data showed in Figs. 2(a)–2(d) for a semi-circular imperfection of diameter. (a) 10 nm, (b) 25 nm, (c) 50 nm and (d) 100 nm. The dashed line shows the width in the absence of the tip.

is smaller than the tip, the profiles may assume the geometry of the apex of the tip [Fig. 2(a)]. However, as the approaching angle increases, there is an (asymmetric) increasing of the optical profile width [Fig. 2(a)]. Such an effect was more clearly seen in the case of the 25 nm diameter semi-circular imperfection [Fig. 2(b)]. There, one can observe that the evolution of the intensity profile with distance (with respect to the origin) moves to the left-hand side as the probe-sample interaction area becomes larger. Here, it is important to note that the increase of such interaction area results in a loss of lateral resolution. The left lateral shift is also present in the optical response of the 50 nm and 100 nm diameters [Figs. 2(c) and 2(d)]. This fact does not play a minor role since one of the most important checks for the validity of an a-SNOM measurement is a precise topography correspondence of the optical contrast.

We measured the width (FHWM) of the intensity profiles showed in Figs. 3(a)–3(d) in order to study the resolution of the proposed system.

It can be noted that the illuminated 10 nm semi-circular imperfection, in general, exhibited an optical profile with a FHWM larger than the spatial dimensions of the imperfection [Fig. 3(a)]. This is expected as the lateral spatial resolution is given by the size of the apex radius. However, a variation of the optical signal is generated once the probe-sample interaction angle is varied even if the probe is located at a fixed vertical position. In the case of the 25 nm semi-circular imperfections, the

illuminated imperfection generated a strong (near-field) focusing which exhibited an optical profile with a FHWM smaller than the spatial dimensions of the imperfection as shown in dashed lines in Fig. 3(b). In this context, Fig. 3(b) shows the width of optical profiles which increases as the value of the angle grows. We can see that the measured width, in the presence of a tip, is smaller than the one obtained without it, due to the probe dimensions. An overall similar resolution effect was obtained when the diameter size was doubled [Fig. 3(c)]. In the next case (100 nm diameter), the evolution of the intensity profile with distance still present and shifts to the left-hand side as the probe-sample interaction angles increases [Fig. 3(d)]. It is clear that for small values, the interaction angle is not as influential as in the previous cases, and it only affects the contrast in the obtained image as expected for a passive probe,[29] where the detection process is linear. The effects begin to enter into play at relative large interaction angles [Fig. 3(d)], i.e. when the interaction area between sample and probe is also large. An interaction angles bigger than 10° is definitely not the best situation in an a-SNOM system since the large interaction area may produce extra artifacts such as mechanical perturbations that causes instability of the probe vibration resulting in a severe changing of the s-SNOM image contrast.[30] In this case, one should also bear in mind that a 100 nm size surface defect may be considered as a relatively large imperfection for many a-SNOM studies.[31] Large size imperfections, in SNOM configurations, are shown to be one of the sources of artifacts in the detected optical signal[32] and therefore they should be treated separately, which is beyond the object of this report.

3.1. *Rectangular imperfection*

As it was aforementioned, we performed a second experiment of the effect of the interaction angle on the optical profiles. In this case, we used a rectangular imperfection. As in the previous analysis, the calculated optical profile showed an evolution of the intensity profile with distance, i.e. the apparent position shifts to the left-hand side [Figs. 4(a)–4(d)], as well as a reduction of the lateral resolution.

Therefore, in Figs. 5(a)–5(d), we show the width of the intensity profiles of Figs. 4(a)–4(d).

It can be seen from Fig. 4(a) that the overall behavior of the optical signal remains similar to that obtained for the smallest semi-circular imperfection. Such a similar behavior can be predicted since the optical signal is dictated by the size of the apex radius. In the following calculations, insets (b) and (c) are the cases for square surfaces imperfections of 12.5 nm and 25 nm of width with 25 nm and 50 nm of height. The results show that the widths changed in a smaller proportion than in the semi-circular imperfection of insets (b) and (c). This is due to the absence of focusing of the field. In the last case [Fig. 5(d)], the contribution of the interaction angle appears to be reduced, at least for the calculated range, because of the relatively large size of the imperfection.

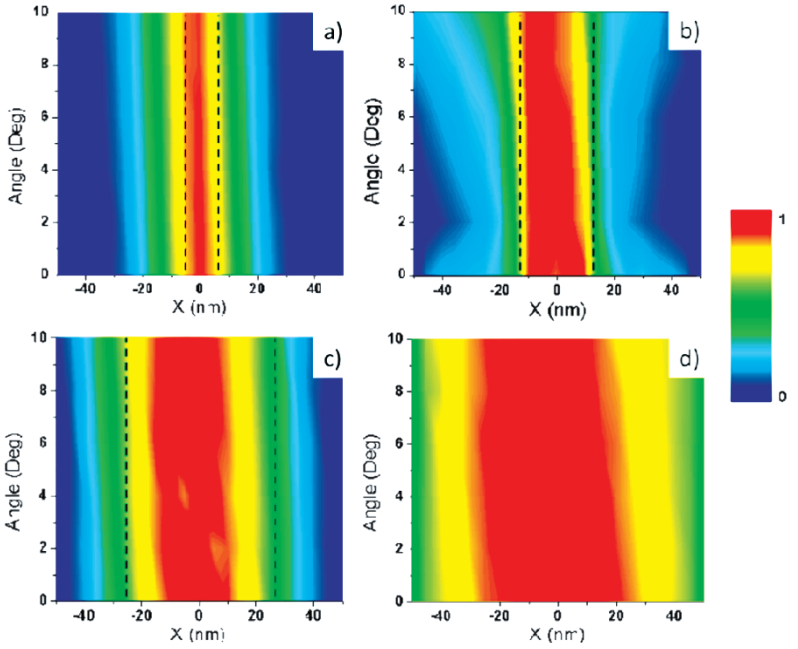

Fig. 4. (Color online) Average intensity obtained at different positions of the X-direction as a function of the interaction angle for a rectangular imperfection of (a) 5×10 nm, (b) 12.5×25 nm, (c) 25×50 nm and (d) 50×100 nm. The dashed lines indicate the width in the absence of the tip. In (d), no dashed line is shown since the width, in the absence of the tip is the whole calculated X profile.

Ideally one would like to relate the optical signal measured along the sample, at a constant altitude, to the unperturbed near-field intensity existing, at the same altitude, and therefore to reconstruct the near field intensity that exists in the absence of the tip, i.e. to reduce the detection process to spatial frequency filtration. However, the a-SNOM mode cannot be realized in its pure form, because the optical responses of the probe tip and sample surface also interact with each other and require one to consider the probe-sample system as a whole.

In general, these series of images evidences the dependence of the resolution on the probe–surface angle interaction in a-SNOM configuration. Such issue may also be present in, for example, AFM techniques. In an AFM the normal interactions have been measured,[33] but in the case of contact mode, there appear lateral forces due to interfacial shear strength which depend of the scan velocity,[34] resulting in the change of the probe-sample interaction angle. Here, an important result is that the calculated optical field profiles have a change in the apparent position to the left-hand side for angles bigger than 6°. Actually, in the square imperfection of Fig. 4(b), the effect is clearer and the position changes 20% in the case of 10°. These last data are more significant if we use dimensional units, i.e. for 10° the change is about 5 nm which is enough to create false information in microscopes

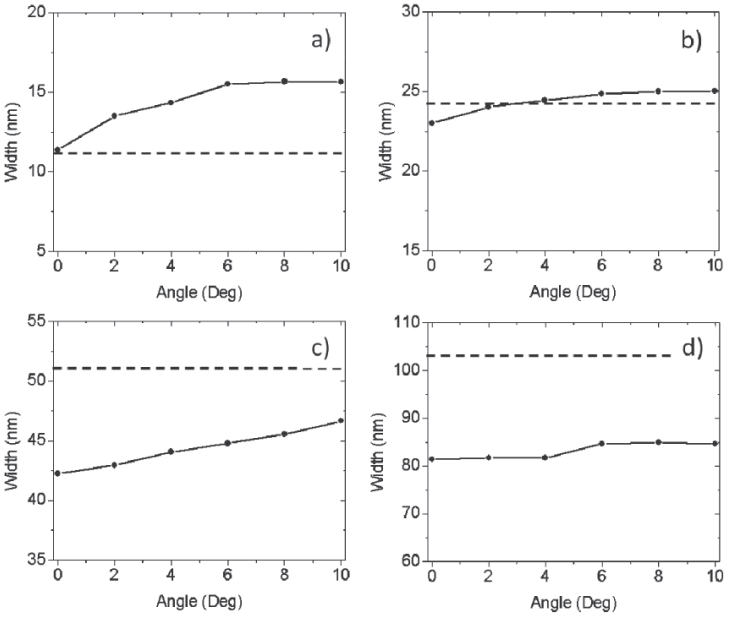

Fig. 5. Normalized width measured at FWHM in data showed in Figs. 4(a)–4(d) for a rectangular imperfection of (a) 5×10 nm, (b) 12.5×25 nm, (c) 25×50 nm and (d) 50×100 nm. The dashed line shows the width in the absence of the tip.

where the lateral resolution is about 15 nm, as in the case of tip-enhanced Raman studies.[35] Furthermore, the resulting effect can be thought of as an analogue of misalignment of the excitation beam in a field enhancing SNOM configuration.[36] Off-apex tip illumination leads to drastic changes in the detected signal because the near field optical tip-sample interaction is essentially turned off.[36] In our case, an increase of the probe-sample interaction angle area would bring, as well, an artifact in the recorded near-field image resolution.

4. Conclusion

We presented the results of a finite-difference time-domain calculation of a probe-sample system illuminated by total internal reflection and operated in constant height mode. It was found that varying the approach angle of the probe with respect to the sample plane introduced artifacts in the near-field optical image. In particular, an angle-dependent shift appears in the image, and an error manifested in a width estimated of several small objects. This was related to the increase of the tip–sample interaction area. This effect causes optical artifacts that may lead to a wrong interpretation of the a-SNOM images. Finally, our work shall continue in the study of the influence of the interaction angle on the optical images obtained by the a-SNOM, in both, three-dimensional FDTD simulations and experimental images.

Acknowledgments

V. Coello acknowledges financial support from CONACyT Project CB-2009-01-127589.

References

1. J. Wessel, *J. Opt. Soc. Am. B* **2** (1985) 1538.
2. U. C. Fischer and D. W. Pohl, *Phys. Rev. Lett.* **62** (1989) 458.
3. F. Zenhausern, Y. Martin and H. K. Wickramasinghe, *Science* **269** (1995) 1083.
4. P. Adam, P. Royer, R. Laddada and J. Bijeon, *Appl. Opt.* **37** (1998) 1814.
5. T. Kalkbrenner, M. Ramstein, J. Mlynek and V. Sandoghdar, *J. Microsc.* **202** (2001) 72.
6. M. Raschke and C. Lienau, *Appl. Phys. Lett.* **83** (2003) 5089.
7. A. Bek, R. Vogelgesang and K. Kern, *Rev. Sci. Instrum.* **77** (2006) 043703.
8. M. Esslinger, J. Dorfmüller, W. Khunsin, R. Vogelgesang and K. Kern, *Rev. Sci. Instrum.* **83** (2012) 033704.
9. F. de Fornel, *Evanescent Waves: From Newtonian Optics to Atomic Optics* (Springer, Heidelberg, 2001).
10. D. Courjon, *Near-Field Microscopy and Near-Field Optics* (Imperial College Press, 2003).
11. E. Betzig, P. L. Finn and J. S. Weiner, *Appl. Phys. Lett.* **60** (1992) 2484.
12. B. Hecht, H. Bielefeldt, Y. Inouye and D. W. Pohl, *J. Appl. Phys.* **81** (1997) 2492.
13. R. Carminati and J. Greffet, *JOSA A* **12** (1995) 2716.
14. V. Coello, S. I. Bozhevolnyi and F. A. Pudonin, *Proc. SPIE* **3098** (1997) 536.
15. J. M. Merlo, J. F. Aguilar, E. Martí-Panameño, R. Cortés and V. Coello, *Rev. Sci. Instrum.* **82** (2011) 083704.
16. A. Banishev, J. Wagner, T. Emig, R. Zandi and U. Mohideen, *Phys. Rev. Lett.* **110** (2013) 250403.
17. M. Labardi, S. Patanè and M. Allegrini, *Appl. Phys. Lett.* **77** (2000) 621.
18. P. G. Gucciardi, G. Bachelier, M. Allegrini, J. Ahn, M. Hong, S. Chang, W. Jhe, S.-C. Hong and S. H. Baek, *Appl. Phys.* **101** (2007) 064303.
19. A. Meixner, M. Bopp and G. Tarrach, *Appl. Opt.* **33** (1994) 7995.
20. K. S. Yee, *IEEE Trans. Antennas Propag.* **14** (1966) 302.
21. M. Kuttge, F. J. García de Abajo and A. Polman, *Opt. Express* **17** (2009) 10385.
22. A. Tatlove, *Computational Electrodynamics: The Finite-Difference Time-Domain Method* (Artech House, Boston, 1995).
23. M. Sipos and B. G. Thompson, *Am. J. Phys.* **76** (2008) 464.
24. F. Toledo-Crow, P. Yang, Y. Chen and M. Vaez-lravania, *Appl. Phys. Lett.* **60**(24) (1992) 15.
25. B. Hecht, B. Sick, U. P. Wild, V. Deckert, R. Zenobi, O. J. F. Martin and D. W. Pohl, *J. Chem. Phys.* **112**(18) (2000) 7761.
26. P. Negrete-Regagnon and E. Mendez, *Meas. Sci. Technol.* **13** (2002) 241.
27. P. B. Johnson and R. W. Christy, *Phys. Rev. B* **6** (1972) 4370.
28. G. Binnig, C. F. Quate and C. Gerber, *Phys. Rev. Lett.* **56** (1986) 930.
29. A. Evlyukhin, G. Brucoli, L. Martín-Moreno, S. I. Bozhevolnyi and F. J. García-Vidal, *Phys. Rev. B* **76** (2007) 075426.
30. D. E. Tranca, C. Stoichita, R. Hristu, S. G. Stanciu and G. A. Stanciu, *Opt. Express* **22** (2014) 1687.
31. R. Carminati and J.-J. Greffet, *Opt. Commun.* **116**(4) (1995) 316.

32. V. Coello, *Surf. Rev. Lett.* **15**(6) (2008) 867.
33. B. Bhushan, *Nanotribology and Nanomechanics* (Springer, New York, 2005).
34. R. W. Stark, G. Schitter and A. Stemmer, *Ultramicroscopy* **100** (2004) 309.
35. T. Ichimura, S. Fujii, P. Verma, T. Yano, Y. Inouye and S. Kawata, *Phys. Rev. Lett.* **102** (2009) 186101.
36. A. Bek, R. Vogelgesang and K. Kern, *Rev. Sci. Instrum.* **77** (2006) 043703.